The 2010 IEEE/RSJ International Conference on
Intelligent Robots and Systems
October 18-22, 2010, Taipei, Taiwan

Optimization and Dynamic Simulation of a Parallel Three Degree–of–Freedom Camera Orientation System

Thomas Villgrattner and Heinz Ulbrich

Abstract— **Information about a user and his intentions can be gained evaluating images acquired from the user's subjective perspective. A possibility to yield high quality images, even under dynamic conditions, is to align a camera with the human gaze direction. Thus, the camera orientation system must cope with the high dynamic human eye movements. Since the system is intended to be head–mounted it must keep small and light. In this paper a spherical parallel manipulator with three degrees–of–freedom is introduced. Beside the kinematic the dynamic model is derived. Furthermore the workspace/package ratio is optimized. To estimate the needed actuator forces and velocities, kinematic and dynamic simulations are carried out. Simulations and measurements obtained with a prototype are presented. Both, simulations and measurements, demonstrate that the device meets the requirements.**

I. INTRODUCTION

The human gaze is one of the most crucial indicators for the direction of spatial and social attention: Information about the user's surroundings, the user's state, and his intentions can be derived from the gaze direction. To gain such information, images from the subjective perspective must be acquired and evaluated. Since users should be able to move freely, the needed cameras must be fixed on the human body or the human head. However, cameras without any supplementary stabilization provide only poor subjective image quality and resolution. To overcome this drawback a head–mounted gaze–driven camera system is presented in [1]. The system continuously tracks the human eye movements and reproduces them with a high speed two degree–of–freedom (DoF) camera orientation device. Since latencies between human eye and camera movements are small enough, the camera orientation device is stabilized by the human vestibulo–ocular and the optokinetic reflexes, without any supplementary post–processing.

Only a few camera orientation systems are known in literature that are able to orient a camera with the desired high dynamics and at the same time are small and lightweight enough to be mounted on a human's head, see [2], [3], and [4]. All these approaches use model aircraft servo actuators. The main drawbacks of these actuators are their unidirectional pulse width modulated (PWM) interface, which introduces a time delay of 20 ms, and their non backlash–free gear boxes. Another small and high–speed camera orientation device with three DoFs is presented in [5]. Because of its low orientation accuracy this device does not suit the application. In this work we extend our previous camera orientation systems, [6] and [7], with two DoF to a system with three DoF. Hence in the following section we will define the requirements and introduce the design of our spherical three DoF camera orientation system. To calculate the accessible workspace, we will deduce the inverse kinematics regarding the joint limitations in Section III. Using parameter variation studies and applying a numerical optimization the workspace will be maximized, while the overall size is kept small. In Section IV we are introducing the dynamic model, used for the actuator selection. Based on the results obtained from the simulations and the optimization processes we assemble a prototype. Using this prototype closed–loop control experiments are performed. The results are presented in Section V. Finally, Section VI is summarizing the paper and will indicate directions of future research.

This work is supported in part within the DFG excellence initiative research cluster "Cognition for Technical Systems – CoTeSys", see also www.cotesys.org.

T. Villgrattner and H. Ulbrich are with the Institute of Applied Mechanics, Technsiche Universität München, Boltzmannstr. 15, 85748 Garching, Germany {villgrattner, ulbrich}@amm.mw.tum.de

II. MECHANICAL DESIGN

The camera orientation device is intended to reproduce the human eye movements. Therefore high velocities and accelerations of up to 500 deg/s and 25000 deg/s^2 and short latencies between user and artificial eye (the camera) movements of about 12 ms are basic system requirements, see [8] and [9]. All three rotational DoF of the human eye must be reproduced and should have a workspace of about ± 20 to ± 30 deg. The angular resolution should be better than 0.02 deg which outreaches the human oculomotor system in extreme gaze fixation by about ten times [10]. Since the system is head–mounted it is important to yield a compact, lightweight and low–noise construction. Of course a high accuracy and backlash–free device is desired.

Due to the requirements of compactness and lightweight only small actuators can be used to drive the camera orientation system. To reach high velocities and accelerations with small actuators it is very important to keep the inertial mass of the moving parts as small as possible. Therefore we chose a design based on a parallel kinematics where the stationary mounted actuators do not perform movements, as in a serial robot, and the inertia of the motors do not add to the inertia of the moving parts. The cost is a more complex mechanism compared to a serial kinematic configuration [11].

Fig. 1 presents a CAD model of our developed camera orientation system. The applied kinematic structure is inspired by the one presented in [12]. However, to suit the application we reduced the size and the weight. Furthermore we use completely different actuator and sensor concepts, to cope with the desired high dynamic movements. Ultrasonic

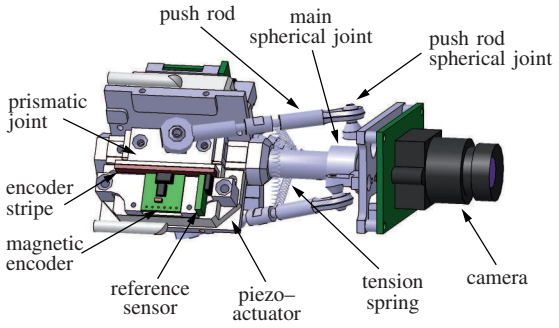

Fig. 1. CAD model of the mechanical setup.

piezo–actuators, P–661 from *Physik Instrumente*, are utilized to drive the camera orientation system. They are small, lightweight and provide high velocities and accelerations. Furthermore they are able to supply high forces also at low speed, so no reduction gear is needed. Each piezo–actuator transmits its movements to a prismatic joint. Small push rods, equipped with spherical joints are attached on the prismatic joints and on the camera frame, forming a so called $\underline{P}SS$ (*p*rismatic, *s*pherical, *s*pherical) chain [12]. The chosen small spherical joints guarantee a high accuracy along their vertical and diagonal axes. To avoid possible backlash around the longitudinal axis the joints are preloaded. Thus, three tension springs connect the push rods with each other. Moreover, the camera frame and the actuator base plate are connected by a passive chain with a spherical joint. Doing so, three rotational DoF are ensured. Because of its central role we call this joint, "main spherical joint". The push rod ends are arranged on a circle with a radius r_1 (actuator base) and r_2 (camera frame) with 120 deg offset between each other. The minimum distance between these two circles is denoted with d, see Fig. 2. To avoid singularities the actuator base and the camera frame are rotated by 60 deg with respect to each other. In order to save space and weight the camera orientation is not directly measured, but calculated from the linear actuator positions. Therefore we attached encoder stripes to the prismatic joints. These stripes can be evaluated by the encoder modules, *SST03* from *Sensitec*, and by the reference sensors, *2SS52M* from *Honeywell*, mounted on the actuator base plate. Besides being small and lightweight this sensor system offer a high resolution of 0.5 µm as well.

III. KINEMATIC DESIGN OPTIMIZATION

To calculate and optimize the workspace of the camera orientation system the nonlinear inverse kinematics is derived. This model does not only take into account the kinematic structure of the system, but also the travel range limitations of the prismatic and spherical joints.

$$\mathbf{q} = \mathbf{g}(\mathbf{w}) \tag{1}$$

Equation (1) denotes the general form of the inverse kinematic model **g**. In the presented case the linear piezo–actuator positions (θ_1, θ_2, and θ_3) correspond to the joint coordinates **q**. The orientation angles (α, β, and γ) correspond to the world coordinates **w**.

Since the inverse kinematic derivation is extensive, the calculations are presented in Appendix I. Using (19) the theoretical desired actuator set points can be calculated from given camera orientation angles. However, the used prismatic and spherical joints provide only a limited operating range. These restrictions are described by (20), (21), and (22), see Appendix II. If these conditions are not fulfilled, the desired orientation angles are out of range.

Nevertheless the reachable workspace depends on the kinematic parameters and on the working range of the employed joints. Accounting for the requirements of compactness and lightweight the joints must be small, but at the same time guarantee a large operational range. In Table I the operating range limits of the selected joints are presented. Once the joints are chosen, the workspace depends on the kinematic parameters only. For the camera orientation device we have defined three parameters, r_1, r_2, and d. As mentioned before the push rod ends are arranged on circles on the actuator base and on the camera frame. The circle radius on the actuator base is depicted with r_1 and r_2 on the camera frame. The minimum length between the two circles is described by d, see Fig. 2. To determine the influence of the different parameters, parameter variation studies are carried out. These studies showed: i) The smaller the circles the pivot points are arranged on, the larger the workspace. ii) The larger the distance between the two circles, the bigger the workspace. The main objective of the optimization process is to yield a small overall size and contemporaneously a large workspace. In case i) both aims can be reached by reducing the two circle radii to a minimum. To guarantee a correct operation of the kinematics, collision between the single components must be avoided. This is accomplished by reducing the radii r_1 and r_2 using the developed CAD model as much as possible. In case ii) the two goals can not be fulfilled at the same time. As stated before, the larger the distance between the two circles, the bigger the workspace. Of course with increasing distance d the overall size increases too. To solve this contradiction we applied a numerical optimization, utilizing an implicit filtering algorithm *IFFCO*. The algorithm is based

TABLE I
OPERATING RANGE LIMITS.

Joint	Limit
Prismatic, θ_{max}	±11 mm
Main spherical, O_{Mmax}	±35 deg
Push rod spherical, O_{PRmax}	±30 deg

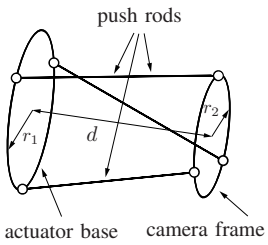

Fig. 2. Kinematic parameters.

on a projected quasi–Newton iteration which uses difference gradients. Fore more information refer to [13].
To maximize the workspace/package dimension ratio the following objective function is chosen:

$$\min f(d) = \min\left(1 - \left(\frac{\mathrm{WS}(d)}{\mathrm{WS}_{max}} - \frac{d}{d_{max}}\right)\right) \qquad (2)$$

During the optimization the distance d between the two circles is varied. For every length the reachable workspace $\mathrm{WS}(d)$ must be calculated. Thus, we gridded the maximum desired workspace WS_{max} with 0.1 deg steps, yielding a set of desired points. A cubic workspace volume with an edge length of ± 30 deg in all three axes is assumed. Afterwards, the single points are checked if they are within the reachable workspace using (19–22). Both values, length between the circles and reachable workspace, are normalized. Though the maximum allowed distance between the two circles is denoted with d_{max} and is chosen to 165 mm. WS_{max} denotes the maximum desired cubic workspace.
For the optimization an initial value of 100 mm was chosen for the length d. The optimization results are presented in Table II. The camera orientation device has an overall size

TABLE II
OPTIMIZATION RESULTS.

Propriety	Value
Covered workspace	84 % of a cubic Volume with ± 30 deg 100 % of a cubic Volume with ± 19 deg
Distance circles, d	40 mm
Radius circle 1, r_1	17 mm
Radius circle 2, r_2	13 mm
Push rod length	42.86 mm
Overall size	$44 \times 44 \times 100\,\mathrm{mm}^3$

of about $44 \times 44 \times 100\,\mathrm{mm}^3$. About 84 % of a cubic workspace volume with ± 30 deg for all three orientations can be covered, see Fig. 3 (left). It is possible to fully cover a cubic workspace volume with about ± 19 deg for all three orientations. If only one orientation is changed at a time and the other two are zero, a workspace of ± 30 deg is covered in the pan and roll orientation, while in the tilt orientation a workspace of ± 29 deg is provided. For a better overview

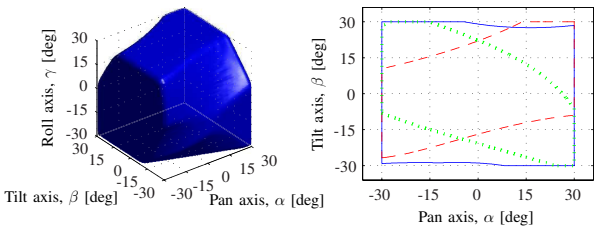

Fig. 3. Covered workspace: 3D (left), slices for neutral [—], maximum [– –], and minimum [· · ·] roll angle (right).

the achievable pan and tilt angles are plotted in Fig. 3 (right) for three different roll orientations. If the roll angle is zero, nearly ± 30 deg can be covered in both, the pan and the tilt orientation. As the plot suggests, the smallest workspace is covered when the roll orientation is either in its maximum or minimum.

To save weight and reduce complexity, the actual camera orientation is calculated from the measured linear actuator positions. Since the relation between actuator positions and camera orientation is nonlinear, the angular resolution is not constant. The maximum quantization error of about 0.0169 deg occurs when the pan, tilt, and roll orientations are in its maximum. Since humans do not orient their eye to such uncomfortable positions very often, see [14], the mean quantization error over the entire workspace was calculated to 0.0067 deg.

IV. KINEMATIC AND DYNAMIC SIMULATIONS

To prove that the selected actuators are able to drive the camera orientation system, a kinematic and dynamic simulation is performed.
In the first step a kinematic model is developed and evaluated. With this model required velocities are estimated. In a second step, a multi–body system is simulated giving access to the entire system dynamics.

A. Kinematic Simulations

To develop a kinematic simulation model we differentiate the inverse kinematic solution (1) with respect to time. Doing so a linear projection between joint and workspace velocities is yield:

$$\dot{\mathbf{q}} = \mathbf{J}^{-1}(\mathbf{w})\dot{\mathbf{w}}. \qquad (3)$$

This kinematic model allows to easily determine the required actuator velocities $\dot{\mathbf{q}}$ over the entire workspace by given angular velocities $\dot{\mathbf{w}}$, with $\mathbf{J}^{-1}(\mathbf{w})$ the systems inverse Jacobian. Since for the desired workspace the manipulator is free of singularities the inverse Jacobian is calculate as follows:

$$\mathbf{J}^{-1}(\mathbf{w}) = \frac{\partial\,\mathbf{q}}{\partial\,\mathbf{w}} = \frac{\partial\,\mathbf{g}(\mathbf{w})}{\partial\,\mathbf{w}}. \qquad (4)$$

$\mathbf{g}$ denotes the inverse kinematic solution, $\mathbf{w}$ the orientation angles, and $\mathbf{q}$ the joint values.
Simulations are carried out to prove that the selected piezo–actuators are able to provide the needed velocities. To simulate the most ambitious case, we chose the fastest human eye movements. These movements are called saccades and can reach velocities of up to 500 deg/s. Investigations reveal that contemporaneous movements around all axes are the most challenging. Thus, saccadic movements around all three axes at the same time are simulated. Doing so for every orientation within the workspace desired velocities are calculated for the single actuators. However, to prove the actuators suitability, only the maximum needed velocities of all actuators must be evaluated. They are introduced in Fig. 4. As this plot suggests, the required maximum actuator velocity is about 260 mm/s. According to the data sheet the actuators are able to provide velocities up to 600 mm/s [15].

B. Dynamic Simulations

For an appropriate actuator selection beside the needed velocities the required accelerations and forces play an important role. While the velocities can be calculated with a kinematic model for the accelerations and forces a dynamic

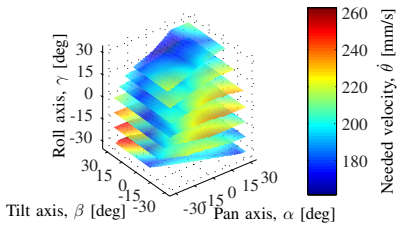

Fig. 4. Kinematic simulation results with constant velocities of 500 deg/s around all three axes.

model is required. To reproduce the entire system behavior our dynamic model accounts for the inertial masses, for the friction in the single joints, and for the tension spring influence. Such a multi body model is derived by the evaluation of the Lagrange or Newton–Euler equations. In the here presented case, we use the multi body simulation tool *MBSim*[1] which is based on a Newton–Euler formalism. Because of the high stiffness and the low weight of the utilized parts, elastic deformation during the motion can be neglected. Therefore the presented parallel kinematics is implemented as a rigid body model and parameterized appropriately. Based on this description *MBSim* is able to internally generate and evaluate the dynamic equations.

The inertia matrices of the single parts, needed for the dynamic model parameterization, can be directly derived from the CAD model. Due to space limitations the inertial matrices are not introduced. However, the masses of the movable parts are presented in Table III. Hereby the mass

TABLE III
MASS MOVABLE PARTS.

Part	Mass
Camera	16 g
Push rod	3 g
Prismatic joint	5 g
Spring	< 0.1 g

TABLE IV
TENSION SPRINGS.

Parameter	Value
m_{TS}	< 0.1 g
$l_{0_{TS}}$	16 mm
c_{TS}	55 N/m

denoted with *Camera* holds the camera, the camera mounting frame and the main spherical joint. The mass denoted with *Push rod* accounts for the push rods itself and for the two attached spherical joints. *Prismatic joint* implies the movable part of the prismatic joints, the linear encoder stripes, and the mounting frame for the encoder stripes. Finally *Spring* denotes the mass of the selected tension springs. Since the spring mass is very small, it is neglected for the simulation. The inertial mass of the *Push rods* and the *Prismatic joints* is considered three times in the dynamic model, once for each piezo–actuator.

As mentioned before the developed *MBSim* model accounts for the tension springs. In Table IV the parameter of the selected springs are listed where the spring mass is denoted by m_{TS}. $l_{0_{TS}}$ describes the unloaded spring length and c_{TS} the spring stiffness.

[1]*MBSim* is an open source **M**ulti **B**ody **Sim**ulation tool which was developed at the Institute of Applied Mechanics, TUM. Is available on http://mbsim.berlios.de/, July 2010.

We used spherical and prismatic joints to setup the camera orientation system. Of course in these joints friction is produced. To decide if this friction must be considered in the dynamic model, we estimated the friction in the single joints.

First the spherical joint influence is calculated with the following equation:

$$M_F \leq C_\alpha \frac{F\, r\, \mu}{\sqrt{1+\mu^2}}, \tag{5}$$

where M_F denotes the frictional torque produced by the spherical joint, C_α is a weighting factor, F describes the force applied to the joint, r denotes the radius of the used ball, and μ is the friction coefficient. A detailed derivation of (5) with more information on the parameters is given in [16].

As mentioned before, we used two different kinds of spherical joints: The main spherical joint and the push rod attached spherical joints. For both the frictional torque is calculated evaluating (5). In Table V the parameters for the friction estimation in the main spherical joint are presented. Ac-

TABLE V
MAIN SPHERICAL JOINT.

Parameter	Value
C_α	1.0
F_{Mmax}	0.87 N
r_M	2.5 mm
μ_M	0.08

TABLE VI
PUSH ROD SPHERICAL JOINT.

Parameter	Value
C_α	1.0
F_{PRmax}	0.65 N
r_{PR}	2.375 mm
μ_{PR}	0.15

cording to [16] the parameter C_α was chosen to be equal to one. F_{Mmax} denotes the maximum applied force to the main spherical joint estimated conducting dynamic simulations. As expected the maximum value arises when the camera is oriented around all three orientations contemporaneously with the maximum velocity. The frictional coefficient between the steel ball and the plastic joint socket is described by μ_M. The maximum friction torque of the main spherical joint was estimated to $M_{F_M} = 0.173 \cdot 10^{-3}$ Nm. To decide if the friction must considered we calculated the needed driving torque in the main spherical joint too. Torques of up to $8.1 \cdot 10^{-3}$ Nm are required to orient a camera with the desired high velocities around all three axes. Thus it can be stated, with respect to the driving torque the small frictional torque can be neglected.

The friction in the spherical joints, attached to the push rods, was calculated in the same way as the friction in the main spherical joint. The parameters for the estimation are listed in Table VI. The maximum frictional torque was calculated to $M_{F_{PR}} = 0.229 \cdot 10^{-3}$ Nm for each of the six joints. We assumed that every piezo–actuator must compensate the friction of two spherical joints. The distance between the point of application of the actuator force and the spherical joint center is 8 mm. Taken into account all these information we calculated the frictional force to 0.057 N. With respect to the driving force, this frictional force is quite small. Hence, it can be neglected.

Each piezo–actuator transmits its movements to the free direction of the prismatic joint. To estimate the induced friction the joint is modeled as a mass–damper element, see Fig. 5.

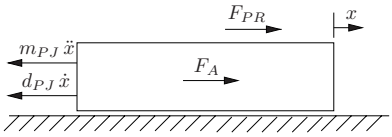

Fig. 5. Mass–damper model of the prismatic joint.

Such a system can be described as follows:

$$m_{PJ}\,\ddot{x} = F_A - d_{PJ}\,\dot{x} + F_{PR}, \tag{6}$$

where m_{PJ} denotes the mass and d_{PJ} the prismatic joint damping coefficient. $\ddot{x}$ and $\dot{x}$ correspond to the prismatic joint acceleration and velocity respectively. F_A denotes the actuator force needed to drive the system and F_{PR} the force induced in the push rods.

We evaluated (6) to calculate the required actuator force, considering the influence of the prismatic joints. Table VII reports the parameters for the simulation. m_{PJ} accounts for

TABLE VII
FRICTIONAL FORCE: PRISMATIC JOINTS.

Parameter	Value
m_{PJ}	5 g
d_{PJ}	1.5 Ns/m

the prismatic joints and for the custom made moving parts. This mass is obtained from the CAD model and from the data sheet respectively. Alike the damping coefficient d_{PJ} was taken from the data sheet. To fulfill the requirements a camera must be oriented with high dynamic movements by the presented kinematics. For this purpose high velocities and accelerations of the linear actuators are required. The conducted simulations confirmed that the frictional force in the prismatic joint plays an important role. Therefore this influence is considered in the dynamic simulation model.

To summarize, we developed and parameterized a dynamic simulation model using *MBSim*. This model accounts for the inertial masses of the single components and for the tension spring influence. We also estimated the friction in the different joints. These calculations demonstrate that the frictional influence of the spherical joints is negligible. However, the friction in the prismatic joint is quite large. Consequently the prismatic joint influence has to be taken into account in the dynamic model.

We carried out different simulations with the implemented dynamic model. Since saccadic eye movements pose the strongest requirements to the system, the following investigations concentrate on this motion pattern. Simulations demonstrate the bigger the simulated saccades and the more DoF involved, the higher the requirements posed to the actuators. For that reason we present simulations were all three DoF change simultaneously over the entire reachable workspace. In such a case a cubic workspace with an edge length of ± 19 deg is covered. We use sinusoidal angle changes to imitate the human eye acceleration and decelerations phases, see Fig. 6 (left). In Fig. 6 (middle) the required angular velocities are indicated. They exceed 800 deg/s. Finally, in Fig. 6 (right) the calculated angular accelerations are presented. The simulated saccades peak value reaches about 25000 deg/s^2. The pan and the tilt movements can not be

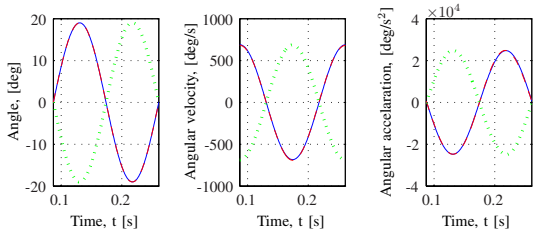

Fig. 6. Desired angles, angle velocities, and angle accelerations around the pan [—], tilt [– –], and roll [· · ·] axis.

distinguished in Fig. 6 because the graphs are superposed in the plots. The roll angle changes with a negative amplitude with respect to the other two orientations. Due to the mechanical design, the actuators must cope with longer travel ranges to fulfill this pattern, compared to a pattern were all angles have the same amplitude. To reach the desired angular velocities and accelerations, both motion patterns must be accomplished in the same time period. Thus, the selected pattern is more challenging for the linear actuators.

The required linear actuator positions, velocities, and accelerations are calculated with the dynamical model using the introduced camera orientation changes. The results are presented Fig. 7. As the plot suggests the requirements to the

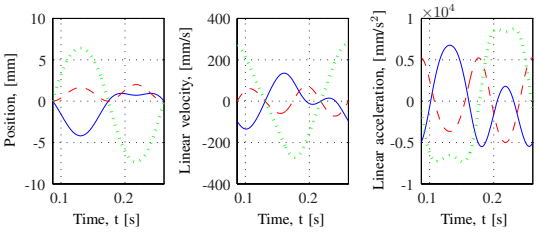

Fig. 7. Desired positions, linear velocities, and linear accelerations of actuator one [—], two [– –], and three [· · ·].

third actuator are the strongest. Maximum velocities of up to 270 mm/s (see Fig. 7 (middle)) and maximum accelerations of up to 8740 mm/s^2 (see Fig. 7 (right)) are required. According to the data sheet [15] both, the velocities and the accelerations, can be supplied by the selected actuators. On the left side of Fig. 8 the calculated actuator forces are present. Compared to the remaining two actuators, the third actuator must fulfill longer travel ranges in the same time period, (see Fig. 7 (left)). Thus higher accelerations are necessary, which yields in the highest force changes. However, the maximum absolute force of about 0.7 N must be supplied by the first actuator. The simulation results

presented in Fig. 8 confirm further that only negative forces must be provided by the piezo–actuators. As stated, to avoid backlash we connected the single push rods with each other using tension springs. Thus, the push rods are tightening together and so the camera tends to rotate clockwise around the longitudinal axis. To inhibit this rotation a negative force must be applied by the actuators. On the right side of Fig. 8

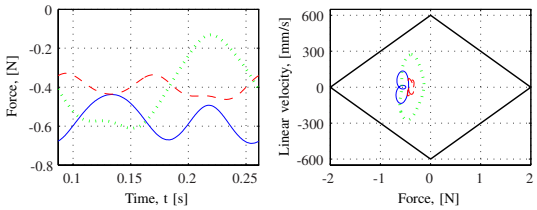

Fig. 8. Desired forces (left), force/velocity diagram (right) of actuator one [—], two [– –], and three [· · ·].

a force/velocity diagram is presented. Here the outer rhomb (bold line) illustrates the piezo–actuators limits according to the data sheet. Inside this rhomb three graphs are presented which introduce the requirements posed to the actuators. This simulation suggests that the actuator maximum capabilities are higher than the required ones.

Based on these investigations and the information obtained from the data sheet we can confirm that the selected piezo–actuators are able to orient a camera with the needed high dynamic movements. However, in the presented considerations model inaccuracies and the negative influence of the lightweight signal cable for the camera are neglected. As confirmed with experiments, the actuator power reserve is high enough to cope with these inaccuracies. Note further, that for the simulation saccades with an amplitude of 38 deg were assumed. According to [17] the amplitude of more than 90 % of the human saccadic eye movement are within 20 deg, which represents lower requirements to the system than the presented one.

V. EXPERIMENTAL EVALUATION

A. Device Setup

Based on the data obtained from the simulations and optimization process, we set up a prototype. A picture of the developed camera orientation system is presented in Fig. 9. The system has a size of 44 × 44 × 100 mm^3 including

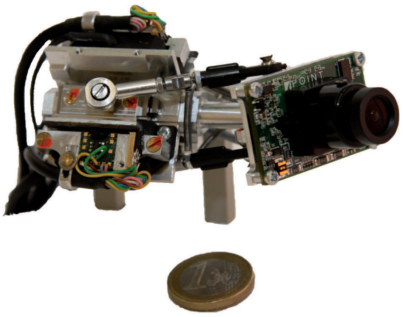

Fig. 9. Three DoF camera orientation system.

the used *Point Grey Firefly MV* camera and an approximate weight of 100 g (without wiring). The mass of the movable parts, including the camera's 11 g, is about 40 g. The camera orientation device covers about 84 % of a cubic workspace volume with ±30 deg for all three orientations. As presented in the next section, angular velocities of over 1000 deg/s can be reached. To save weight and reduce complicity the camera orientation is calculated from measured linear actuator positions. Due to the nonlinearity in the kinematic solution, the angular resolution is not constant. For the developed system the maximum quantization error is about 0.0169 deg. The main parameters of the developed system are summarized in Table VIII.

TABLE VIII
SPECIFICATIONS OF THE THREE DOF CAMERA ORIENTATION SYSTEM.

Propriety	Value
Covered workspace	84 % of a cubic Volume with ±30 deg 100 % of a cubic Volume with ±19 deg
Angular velocities	> 1000 deg/s
Maximum quantization error	0.0169 deg
Mean quantization error	0.0067 deg
Overall size*	44 × 44 × 100 mm^3
Push rod length	42.86 mm
Overall mass*	100 g
Mass movable parts*	40 g

* The presented values do not account for cabling.

B. Experimental Results

To prove that the developed prototype is able to orient a camera with the required high dynamic orientation changes, closed–loop control experiments were performed. We introduced the used joint space control architecture in [18]. Thus, here only a brief overview of the architecture and exemplary control results are presented.

In the chosen control approach the desired camera orientation is transformed to linear actuator set points using the inverse kinematics. These positions are adjusted with three separated closed–loop proportional-integral (PI) controllers.

To imitate the fastest human eye movements (saccades), step response measurements were performed, while the pan orientation changes from 20 deg to -20 deg and the tilt and roll angles are set to zero. Fig. 10 (left) reveals that the new

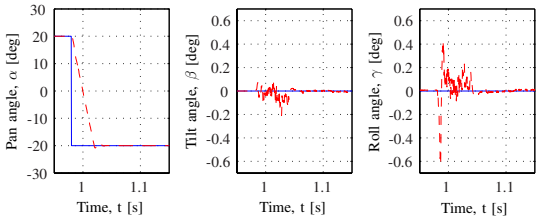

Fig. 10. Desired [—] and actual [– –] orientation during step response.

orientation can be reached in about 40 ms, which results in a fast angular movement of about 1000 deg/s, with only a small overshooting of about 2 %. In addition an angular orientation error in the tilt axis of about 0.2 deg and in the roll axis of

about 0.6 deg can be registered. These errors occur because of the parallel structure of the kinematic system. Position errors arising during displacement of at least one of the linear axes always results in angular errors of all orientations. The presented measurements were preformed while the maximum achievable velocity was artificially limited to 1000 deg/s. Doing so the required velocities of 500 deg/s can be provided and the errors in the non tilted axes are reduced. Experiments without this limitation revealed that it is possible to reach an average velocity of more than 2500 deg/s around the roll axis.

VI. CONCLUSIONS AND FUTURE WORK

In this paper we presented and verified the design and optimization of a three DoF spherical kinematics. Due to the planned application, as a part of a gaze–driven head–mounted camera system or as an artificial eye for humanoid robots, the device must cope with the high dynamic orientation changes of the human oculomotor system and at the same time be small and light in weight. Therefore our suggested approach is based on a piezo–actuator driven parallel kinematic structure. To determine the workspace we derived the inverse kinematics accounting for the different joint limitations. The workspace/package dimension ratio was maximized using an implicit filtering algorithm. About 84 % of a cubic workspace volume with an edge length of ± 30 deg for all three orientations is covered. Our camera orientation device has a size of $44 \times 44 \times 100\,\mathrm{mm}^3$ and a weight of about 100 g. Beside a kinematic a dynamic simulation model was derived. The latter accounts for the inertial mass and the friction of the single parts. We carried out simulations with these models, using special motion patterns. Also for saccades, which can be considered as the most challenging eye movements, the selected piezo–actuators suit the application. The simulation results were confirmed with closed–loop control experiments. Thus it can be stated, that the developed camera orientation system is able to outreach the capabilities of the human oculomotor system. Beside supplementary tests, the integration in a head–mounted gaze–driven camera system and in a humanoid robot head is planned.

The investigated kinematics could also be used for other duties, e.g. as a wrist joint for robotic applications, as tool holder in CNC machines, or as orientation system for bigger cameras. Based on our kinematic models, the workspace of the devices can be optimized, with respect to the overall size, potential singularities, and quantization errors. The expected actuator forces can be calculated using our dynamic models. Thus, for further applications the design optimization and comparison of different kinematic parameters as well as actuators can be effectively handled.

APPENDIX I: INVERSE KINEMATICS

In this section we introduce the inverse kinematic solution. Fig. 11 presents the kinematic scheme and the nomenclature used for the calculations. Both introduced coordinate systems have their origin in the center of the main spherical joint (bold in Fig. 11). $\mathbf{S}_0$ denotes the base coordinate system and $\mathbf{S}_{Cam}$ the camera fixed coordinate system. Fig. 11 presents the mechanism in its neutral position, whit all camera angles and actuator positions equal to zero. In this case the two coordinate systems correspond and the z–axes coincide with the cameras optical axis. All y–axes face to the right and the x–axes upwards.

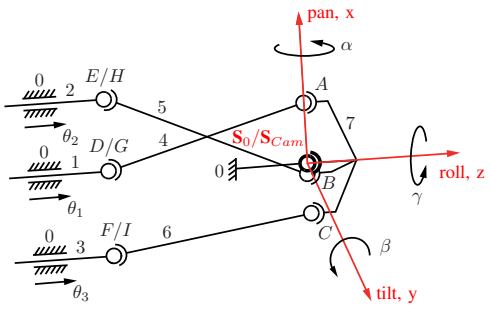

Fig. 11. Kinematic scheme.

With three vectors we describe the spherical joint center points A, B, and C in the camera attached coordinate system $\mathbf{S}_{Cam}$ as follows:

$$ {}_{Cam}\mathbf{a} = [{}_{Cam}a_x,\ {}_{Cam}a_y,\ {}_{Cam}a_z]^T, \tag{7} $$

$$ {}_{Cam}\mathbf{b} = [{}_{Cam}b_x,\ {}_{Cam}b_y,\ {}_{Cam}b_z]^T, \tag{8} $$

$$ {}_{Cam}\mathbf{c} = [{}_{Cam}c_x,\ {}_{Cam}c_y,\ {}_{Cam}c_z]^T. \tag{9} $$

The constant vectors are transformed into the base coordinate system $\mathbf{S}_0$ using the homogeneous rotation matrix:

$$ {}^0\mathbf{R}_{Cam} = (Rot({}_{Cam}z, \gamma) Rot({}_{Cam}y, \beta) Rot({}_{Cam}x, \alpha))^T, \tag{10} $$

where α denotes a rotation around the camera's vertical axis (pan), β a rotation around the horizontal axis (tilt), and γ a rotation around the longitudinal axis (roll). With this transformation we write:

$$ {}_0\mathbf{a} = {}^0\mathbf{R}_{Cam}\ {}_{Cam}\mathbf{a} = [{}_0a_x,\ {}_0a_y,\ {}_0a_z]^T, \tag{11} $$

$$ {}_0\mathbf{b} = {}^0\mathbf{R}_{Cam}\ {}_{Cam}\mathbf{b} = [{}_0b_x,\ {}_0b_y,\ {}_0b_z]^T, \tag{12} $$

$$ {}_0\mathbf{c} = {}^0\mathbf{R}_{Cam}\ {}_{Cam}\mathbf{c} = [{}_0c_x,\ {}_0c_y,\ {}_0c_z]^T. \tag{13} $$

The spherical joint center points G, H, and I attached to the prismatic joints are described with the following vectors:

$$ {}_0\mathbf{g} = [{}_0d_x,\ {}_0d_y,\ {}_0d_z + \theta_1]^T, \tag{14} $$

$$ {}_0\mathbf{h} = [{}_0e_x,\ {}_0e_y,\ {}_0e_z + \theta_2]^T, \tag{15} $$

$$ {}_0\mathbf{i} = [{}_0f_x,\ {}_0f_y,\ {}_0f_z + \theta_3]^T, \tag{16} $$

where ${}_0d_i$, ${}_0e_i$, and ${}_0f_i$ $(i = x, y, z)$ are the components of the constant vectors ${}_0\mathbf{d}$, ${}_0\mathbf{e}$, and ${}_0\mathbf{f}$ describing the actuators neutral position. The actuator displacement is described with θ_i $(i = 1, 2, 3)$. To afford a symmetrical design the length l of all three push rods is equal. For the first push rod, between the points A and G, we describe this length as follows:

$$ l = |{}_0\mathbf{a} - {}_0\mathbf{g}|, \tag{17} $$

where ${}_0\mathbf{a}$ denotes the vector to the point A and ${}_0\mathbf{g}$ to the point G. With the following abbreviations:

$$ \Delta x_1 = {}_0a_x - {}_0d_x, \quad \Delta y_1 = {}_0a_y - {}_0d_y, \quad \Delta z_1 = {}_0a_z - {}_0d_z, $$

$$ \Delta l_1^2 = l^2 - \Delta x_1^2 - \Delta y_1^2 - \Delta z_1^2, \tag{18} $$

and after solving the quadratic equation, θ_1 is calculated:

$$ \theta_{1_{1,2}} = \Delta z_1 {}^{(}\pm{}^{)} \sqrt{\Delta z_1^2 + \Delta l_1^2}. \tag{19} $$

θ_2 and θ_3 are calculated in the same way as θ_1 by simply replacing the vectors ${}_0\mathbf{a}$, ${}_0\mathbf{d}$, and ${}_0\mathbf{g}$ in (17) and (18). Accounting for the limitations of the piezo–actuator's travel range

$$|\theta_i| \leq \theta_{max}, \qquad i = 1, 2, 3, \tag{20}$$

where θ_{max} denotes the maximum piezo–actuator travel range, confirms that only one solution is possible. Considering the kinematic structure we put the "plus sign" in (19) in brackets, because it belongs to the assembly variation disregarded in this article.

APPENDIX II: JOINT RESTRICTIONS

In this section we present the influence of the joint limitations on the workspace. Considering the actuator travel range restrictions is quite simple. The required actuator positions must fulfill (20), otherwise the desired orientation angles are out of range.

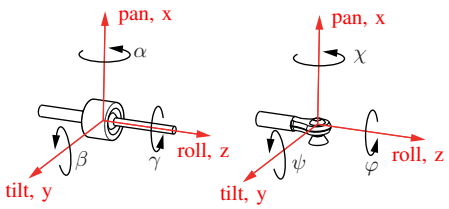

Fig. 12. Main spherical joint (left), push rod spherical joint (right).

On the left side of Fig. 12 the main spherical joint is illustrated. This joint is mounted in the base coordinate system origin. Thus, it will be oriented in the same direction as the camera. The maximum deflection in both the pan and the tilt orientation can be achieved independently. The roll orientation has no restrictions. These relations are described as follows:

$$|\alpha| \leq O_{Mmax}, \qquad |\beta| \leq O_{Mmax}, \tag{21}$$

where α describes the pan and β the tilt orientation of the camera. O_{Mmax} depicts the maximum reachable orientation angle of the main spherical joint. The by the joint provided deflections ($\pm$35 deg, see Table I) are greater than the maximum desired ones ($\pm$30 deg). Therefore the achievable workspace is not restricted by the main spherical joint.

In Fig. 12 (right) a spherical joint attached to the push rods is presented. We denote the orientation around the vertical axis (pan) with χ, around the diagonal axis (tilt) with ψ, and around the longitudinal axis (roll) with φ. Rotations around the pan axis of these joints are free of restrictions. However, deflections in the remaining two orientations are limited. Due to the spherical joint design, the achievable orientation around the tilt axis depends on the actual roll orientation (and vice versa). We describe these relations as follows:

$$\left|\sqrt{\psi^2 + \varphi^2}\right| \leq O_{PRmax}, \tag{22}$$

The maximum achievable orientation is denoted with O_{PRmax}. Depending on the parameters (e.g. the push rod length) an initial spherical joint deflection arises and so the workspace is limited. Thus, we calculate and compensate the initial joint deflections in the mechanism's neutral position for every investigated configuration. Afterwards the spherical joint deflections are calculated over the entire workspace. Note that a desired camera orientation is only achievable if (22) is fulfilled for all six push rod spherical joints. Due to limitations of space we omit the detailed derivation of the spherical joint orientations, ψ and φ.

ACKNOWLEDGMENTS

The authors appreciate the valuable comments by the anonymous reviewers, which helped to strengthen the paper considerably. Special thanks go to M. Schneider for his support during the setup of the multi body simulation model. The authors would also like to thank E. Schneider from the Chair for Clinical Neurosciences, Ludwig-Maximilians Universität München, for the fruitful discussions.

REFERENCES

[1] E. Schneider, T. Villgrattner, J. Vockeroth, K. Bartl, S. Kohlbecher, S. Bardins, H. Ulbrich, and T. Brandt, "Eyeseecam: An eye movement–driven head camera for the examination of natural visual exploration," *Annals of the New York Academy of Sciences*, vol. 1164, no. Basic and Clinical Aspects of Vertigo and Dizziness, pp. 461–467, 2009.

[2] W. W. Mayol, B. J. Tordoff, and D. W. Murray, "Wearable visual robots," in *Proc. Fourth International Symposium on Wearable Computers*, 16–17 Oct. 2000, pp. 95–102.

[3] E. Schneider, T. Dera, K. Bard, S. Bardins, G. Boening, and T. Brand, "Eye movement driven head-mounted camera: it looks where the eyes look," in *IEEE International Conference on Systems, Man and Cybernetics, 2005*, vol. 3, 2005, pp. 2437–2442 Vol. 3.

[4] P. Wagner, W. Günthner, and H. Ulbrich, "Design and implementation of a parallel three-degree-of-freedom camera motion device," in *Proceedings of Joint Conference of the 37th International Symposium on Robotics ISR 2006 and the German Conference on Robotics*, Munich, Germany, May 2006, pp. 1–12.

[5] M. Hoshina, T. Mashimo, and S. Toyama, "Development of spherical ultrasonic motor as a camera actuator for pipe inspection robot," in *IEEE/RSJ International Conference on Intelligent Robots and Systems, 2009. IROS 2009.*, St. Louis, MO, USA, Oct. 2009, pp. 2379–2384.

[6] T. Villgrattner and H. Ulbrich, "Design and control of a compact high–dynamic camera–orientation system," *IEEE/ASME Transactions on Mechatronics*, vol. in press, no. 99, pp. 1–11, 2010.

[7] T. Villgrattner, T. Thümmel, and H. Ulbrich, "Light-weight high dynamic camera orientation system," in *Proceedings of the 5th International Workshop on Computational Kinematics*, A. Kecskeméthy and A. Müller, Eds. Springer, June 2009, pp. 307–314.

[8] J. R. Leigh and D. S. Zee, *The neurology of eye movements*, 4th ed., ser. Contemporary neurology series. Oxford University Press, Inc. New York, Apr. 2006, vol. 70.

[9] B. D. Corneil, C. A. Hing, D. V. Bautista, and D. P. Munoz, "Human eye–head gaze shifts in a distractor task. i. truncated gaze shifts," *Journal of Neurophysiology*, vol. 82, no. 3, pp. 1390–1405, Sep 1999.

[10] T. J. Brunstetter, G. L. Mitchell, and N. Fogt, "Magnetic field coil measurements of the accuracy of extreme gaze ocular fixation." *Optometry and Vision Science*, vol. 81, no. 8, pp. 606–615, Aug 2004.

[11] S. Riebe and H. Ulbrich, "Modelling and online computation of the dynamics of a parallel kinematic with six degrees-of-freedom," *Archive of Applied Mechanics (Ingenieur Archiv)*, vol. 72, no. 11, pp. 817–829, Jun 2003.

[12] J. Merlet, *Parallel Robots*, ser. Solid Mechanics and Its Applications, G. Gladwell, Ed. Kluwer Academic Publishers, 2000, vol. 74.

[13] P. Gilmore and C. Kelley, "An implicit filtering algorithm for optimization of functions with many local minima," *Journal of Optimisation (SIAM)*, vol. 5, pp. 269–285, 1995.

[14] M. B. 't Hart, J. Vockeroth, F. Schumann, K. Bartl, E. Schneider, P. König, and W. Einhäuser, "Gaze allocation in natural stimuli: Comparing free exploration to head–fixed viewing conditions," *Journal of Visual Cognition*, vol. 17, no. 6, pp. 1132–1158, 2009.

[15] Physik Instrumente (PI) GmbH & Co. KG, *MP 76E User Manual, P–661, PILine®OEM Piezo Linear Motors*, 1st ed., Feb. 2006.

[16] A. Faraz and S. Payandeh, "Towards approximate models of coulomb frictional moments in: (i) revolute pin joints and (ii) spherical-socket ball joints," *Journal of Engineering Mathematics*, vol. 40, pp. 283–296(14), 2001.

[17] R. H. S. Carpenter, *Movements of the Eyes*, 2nd ed. London: Pion Ltd, 1998.

[18] T. Villgrattner, E. Schneider, P. Andersch, and H. Ulbrich, "Compact high dynamic 3 dof camera orientation system: Development and control," in *Proceedings of The 10th International Conference on Motion and Vibration Control (MOVIC 2010)*, Tokyo, Japan, Aug. 2010, pp. 1–10, in press.